

H₃PW₁₂O₄₀ Anchored on the Three-Dimensional and Networked SBA-15 as an Efficient and Recyclable Catalyst for Mannich Reaction

Tengfei Zhang, Wei Zhang, Hao Dong, Qing Liu*

Key Laboratory of Low Carbon Energy and Chemical Engineering, College of Chemical and Environmental Engineering, Shandong University of Science and Technology, Qingdao Shandong 266590, China.

*Corresponding author: Qing Liu, email: qliu@sdust.edu.cn

Received July 22th, 2019; Accepted August 21th, 2019.

DOI: <http://dx.doi.org/10.29356/jmcs.v64i1.1034>

Abstract. The three-dimensional and networked SBA-15 (3D-SBA-15) supported phosphotungstic acid (PW) was used as heterogeneous catalyst for the one-pot three-components Mannich reaction at room temperature. The H₃PW₁₂O₄₀/3D-SBA-15 catalyst was prepared using an impregnation method and confirmed by series of characterizations such as Fourier-transform infrared spectra (FT-IR), scanning electron microscope (SEM), transmission electron microscopy (TEM), X-ray diffraction (XRD), N₂ physisorption and thermogravimetric (TG) analysis. 50PW/3D-SBA-15 catalyst with H₃PW₁₂O₄₀ loading of 50 wt% showed the highest yield of 93% in 1.8 h for the Mannich reaction of benzaldehyde, aniline and acetophenone under solvent-free condition. A series of β -aminoketone derivatives were synthesized successfully in the presence of this catalyst. In addition, H₃PW₁₂O₄₀/3D-SBA-15 catalyst can be easily recovered and reused four times without significant decrease of the activity. This work provides an improved modification of the three-component Mannich reaction in terms of mild reaction conditions, clean reaction profiles, small quantity of catalyst and a simple workup procedure.

Keywords: H₃PW₁₂O₄₀; 3D-SBA-15; heterogeneous catalysis; Mannich reaction.

Resumen. El ácido fosfotungstico (PW) se soportó en sílice SBA-15 (3D-SBA-15) y se usó como catalizador heterogéneo en la reacción de Mannich en un solo paso de tres componentes a temperatura ambiente. El catalizador H₃PW₁₂O₄₀/3D-SBA-15 se preparó mediante impregnación y se caracterizó por espectroscopia de infrarrojo (FT-IR), microscopía electrónica de barrido (SEM), microscopía electrónica de transmisión (TEM), difracción de rayos-X (XRD), fisisorción de N₂ y análisis termogravimétrico (TG). El catalizador 50PW/3D-SBA-15, con una carga de H₃PW₁₂O₄₀ del 50% en peso, mostró el rendimiento más alto del 93% en 1.8 h para la reacción de Mannich entre benzaldehído, anilina y acetofenona, sin disolvente. Se sintetizó una serie de derivados de β -aminocetona en presencia de este catalizador. Además, el catalizador H₃PW₁₂O₄₀/3D-SBA-15 puede recuperarse fácilmente y reutilizarse cuatro veces sin pérdida significativa de la actividad. Este trabajo reporta una modificación de la reacción de Mannich de tres componentes bajo condiciones de reacción suaves, perfiles de reacción limpios, pequeña cantidad de catalizador y un procedimiento de tratamiento simple.

Palabras clave: H₃PW₁₂O₄₀; 3D-SBA-15; catálisis heterogénea; reacción de Mannich.

Introduction

Green chemistry has played an important role in protecting human health and the environment in an economically beneficial manner in many fields, such as catalysis, the design of safer chemicals and

environmentally benign solvents [1-3]. Among them, the application of heterogeneous catalysts in place of homogeneous catalysts in organic synthesis is an attractive area of research in the laboratory as well as in industry [4, 5].

Mannich reaction is an important reaction to produce β -amino carbonyl compounds, which can be catalyzed by some acidic catalysts. However, these strategies suffer from several shortcomings, such as low yields [6], long reaction times [7], and the use of environmentally unfriendly solvents [8]. Therefore, there is high interest in developing new catalysts to overcome the drawbacks of the classical methods [9].

Heteropoly acids (HPAs), especially those of the Keggin series, are widely used under both homogeneous and heterogeneous as catalysts for the synthesis of fine and specialty chemicals [10, 11]. HPAs show the very strong Brønsted acidity values, approaching the super acid region [12]. Due to their stronger acidity, they generally exhibit higher catalytic activities than conventional catalysts, such as mineral acids, ion-exchange resins, zeolites, etc. in both heterogeneous and homogeneous systems. As found recently, Keggin-type heteropoly acids, e. g., $H_3PW_{12}O_{40}$, have been extensively studied because they are highly solid acid catalysts in homogeneous system [13-15].

Ordered mesoporous materials with large surface areas and controlled specific morphologies have drawn great attention in catalysis as well as in materials science [16]. Silica-based mesoporous materials such as SBA-15, KIT-6 and MCM-41 etc. [17-19] have been widely reported. Among them, the textural properties of SBA-15 can be altered in a wide range and various morphologies, such as rod, fiber, sphere, film, monolith, etc. [20-22]. Zhou et al. successfully synthesized 3D-SBA-15 with net-linked microscopic structure by controlling the shearing force and the acidity of the system [23]. Liu et al. prepared NiO/3D-SBA-15 catalyst by one-pot method for CO_2 methanation and found that higher Ni dispersion and more Ni particles dispersed in the meso-channels [24]. Yang et al. prepared a Co_3O_4 - CeO_2 functionalized 3D-SBA-15 monolith by isovolumetric impregnation improves NO_x -assisted soot combustion. It was revealed that, compared with unsupported Co_3O_4 - CeO_2 particles, the CoCe/3D-SBA-15 catalysts with optimized Co_3O_4 - CeO_2 loading showed much higher catalytic ability, achieving a complete oxidation of the soot to CO_2 below 400 C in the presence of NO_x , which is attributed to the high dispersion of Co_3O_4 - CeO_2 on 3D-SBA-15 and the cross-linked macroporous structure of 3D-SBA-15 that can house the soot particulates, thus providing closer contact between the soot and catalytically active sites [22]. Therefore, 3D-SBA-15 is one of the most attractive catalyst supports because of the high specific surface area, unique spatial structure, which allows the active components to be better dispersed.

To overcome the above mentioned problems of Mannich reaction, a new $H_3PW_{12}O_{40}$ /3D-SBA-15 catalyst was used in this work. The high specific surface area of 3D-SBA-15 facilitates the high dispersion of active component to generate more active sites, while the macropores derived from the 3D network of 3D-SBA-15 provide high accessibility of the Mannich reactants to the active sites. This catalyst system is a one-pot procedure achieved under solvent-free conditions, and the catalyst can be recovered to inhibit any contamination to the environment with high activity and recyclability [25].

Experimental

Chemicals and apparatus

Chemicals

Pluronic P123 was purchased from Sigma–Aldrich, and all other chemicals with analytical grade were purchased from Shanghai Macklin Biochemical Co., Ltd, China, which were used without further treatment.

Characterizations

Hammett acidity measurement, 5 mL indicator solution of cyclohexane was added to a weighed sample of PW on silica so that each test sample contained 100 mg silica (total weight varied depending on PW loading). Phenylazoaniline ($H_0 = +2.8$), dicinnamalacetone ($H_0 = -3.0$), benzalacetophenone ($H_0 = -5.6$), anthraquinone ($H_0 = -8.2$), 4-nitrotoluene ($H_0 = -11.35$) and 2,4-dinitrotoluene ($H_0 = -13.75$) were used as Hammett indicators. pH measurement was used a PHS-3C pH meter (INESA Scientific Instrument Co., Ltd).

Elemental analysis was undertaken on a Fisons ICP-OES instrument. The thermogravimetric (TG) analysis was conducted on a thermogravimetric analyzer (TGA 2, Mettler, USA) in air flow (200 mL min⁻¹) from room temperature up to 1000 °C (10 °C min⁻¹). N₂ adsorption was performed on a surface area & pore size analyzer (Quantachrome, NOVA 3200e) at -196 °C. The specific surface area was determined according to the Brunauer-Emmett-Teller (BET) method in the relative pressure range of 0.05–0.3. The pore size distribution was calculated with the Barrett-Joyner-Halenda (BJH) method using the adsorption isotherm branch. The Fourier-transform infrared spectra (FT-IR) were taken on a Nicolet 380 Fourier Transform-Infrared spectrophotometer (Thermo Electron Corporation, USA) in the range of 400–4000 cm⁻¹. X-ray diffraction (XRD) pattern was obtained by a Rigaku Ultima IV (Rigaku Corporation, Osaka, Japan) with a step of 0.02 from 5.0 to 80.0 (wide angle range) using Cu K_α radiation (λ=1.5418 Å) at 40 kV and 40 mA. The sample was checked with the card number of Joint Committee on Powder Diffraction Standards (JCPDS). The morphology of the samples was visualized using an emission scanning electron microscope (SEM) (JSM-6700F, JEOL) [26] and transmission electron microscopy (TEM) (JEM-2010F, JEOL) equipped with an energy-dispersive X-ray spectroscopy (EDS) detector. Melting points (M.p.) were determined by using XT-4 micromelting point apparatus (Beijing Taike Instrument Company, China). ¹H NMR spectra were taken on an EFT-60 NMR spectrometer (Anasazi Instruments, USA) using CDCl₃ as solvent and TMS as the internal standard.

Catalyst preparation

Preparation of 3D-SBA-15

The monolithic 3D-SBA-15 was synthesized according to the method described earlier. Typically [22], 9.13 g Methyl orthosilicate (TMOS) was added dropwise to the already dissolved aqueous solution containing 6.89 g citric acid, 3.00 g P123 block copolymer and 112.00 g deionized water, and the mixture was kept under mild stirring till the monolith-like solid was formed at 40 °C for 24 h. The resulting gel was transferred into a teflon bottle and heated at 100 °C for 24 h. Subsequently, the solid product was recovered by filtration, washed with deionized water, and air-dried at room temperature. To remove the template, the dried monolithic solid was calcined in an air flow at 823 °C for 5 h in a tube furnace.

Preparation of H₃PW₁₂O₄₀/3D-SBA-15

H₃PW₁₂O₄₀ (0.3, 0.5 or 0.7 g) was dissolved in the deionized water (10 mL), and a certain amount of 3D-SBA-15 was added to the solution with strong mixing at 60 °C for 10 h. Then, the 1g catalysts with the loading of 30, 50 and 70 wt% H₃PW₁₂O₄₀ were obtained after the evaporation of solvent at 80 °C and denoted as mPW/3D-SBA-15 (m=30, 50 or 70) in this work.

General procedure for Mannich reaction

Typically, aldehyde (20 mmol) and aromatic amine (20 mmol) were added and stirred in a 50 mL round-bottomed flask at room temperature for 10 min. Then, acetophenone or cyclohexanone (20 mmol), mPW/3D-SBA-15 (0.5 g) were added successively. After completion of the reaction, the mixture was treated with saturated NaHCO₃ solution (10 mL). The product was filtered and washed with water several times and recrystallized from ethanol and acetone (1:1) to afford the pure product.

Results and discussion

Catalyst characterizations

N₂ physisorption

The N₂ adsorption–desorption isotherms of 3D-SBA-15 and mPW/3D-SBA-15 catalysts are shown in Fig. 1. The isotherms of 3D-SBA-15 is type IV and gives hysteresis of type H1 at high relative pressures (P/P₀>0.6), demonstrating typical mesoporous structure formation of 3D-SBA-15. The shapes of isotherms and hysteresis loop of mPW/3D-SBA-15 catalysts are similar to those of 3D-SBA-15, indicating that the ordered mesoporous structure still remains after the loading of H₃PW₁₂O₄₀ into 3D-SBA-15. However, the condensation steps of mPW/3D-SBA-15 (m=30 and 50) become less steep and shift to lower P/P₀ values with the increase of

$\text{H}_3\text{PW}_{12}\text{O}_{40}$ loadings, indicating the occupancy of some pores by $\text{H}_3\text{PW}_{12}\text{O}_{40}$ species in 3D-SBA-15 support after the impregnation, which may result in the decrease of pore diameter. Moreover, 70PW/3D-SBA-15 shows type IV isotherms with H4-type hysteresis loop due to the excess $\text{H}_3\text{PW}_{12}\text{O}_{40}$ loading. The pore size distribution curves of 3D-SBA-15 and mPW/3D-SBA-15 ($m=30$ and 50) are all narrow. The peaks of the mPW/3D-SBA-15 ($m=30$ and 50) curves shift to around 6.0 nm compared with that of 3D-SBA-15 at around 8.0 nm. In contrast, the pore size distribution curve of 70PW/3D-SBA-15 is broader and centered at around 8.0 nm [27]. Table 1 lists the BET surface areas, pore sizes and pore volumes of all the samples. It shows that 3D-SBA-15 exhibits high surface area up to $515.80 \text{ m}^2 \text{ g}^{-1}$, large pore volume up to $0.75 \text{ cm}^3 \text{ g}^{-1}$ and average pore diameter around 5.81 nm. The surface area, pore volume, and average pore diameter of mPW/3D-SBA-15 catalysts are showed in Table 1. As shown, the surface area diminishes linearly, when the mass of $\text{H}_3\text{PW}_{12}\text{O}_{40}$ increases. As we know, the molecular size of $\text{H}_3\text{PW}_{12}\text{O}_{40}$ is about 1.2 nm smaller than the pore size of 3D-SBA-15, which suggests that $\text{H}_3\text{PW}_{12}\text{O}_{40}$ molecule can successfully enter the pores. Thus, the blockage of some pores as well as the decrease of the mass weight of the porous support result in the decrease of these parameters determined by N_2 physisorption.

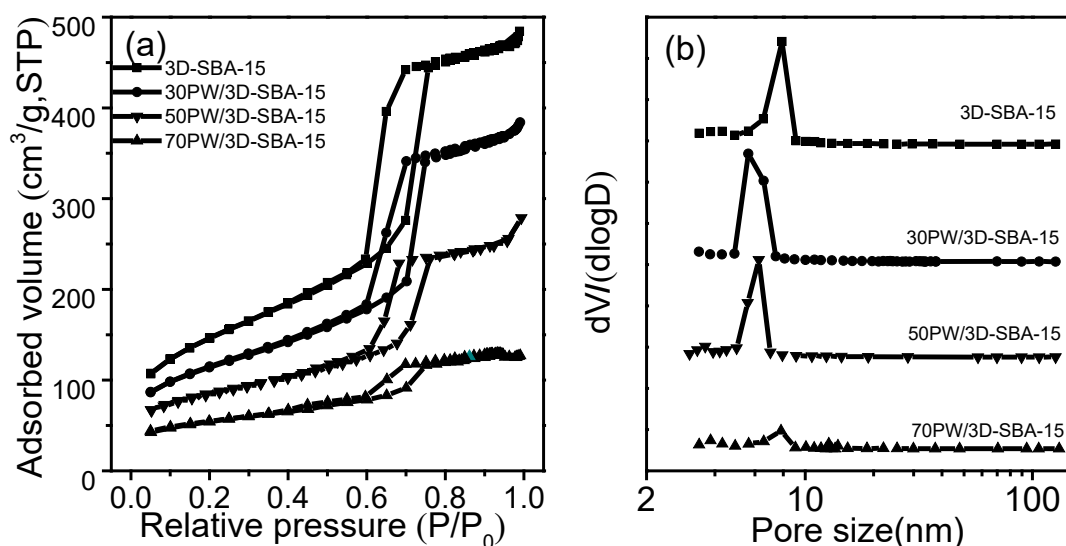


Fig. 1. N_2 adsorption isotherms (a) and pore size distribution curves (b) of 3D-SBA-15 and mPW/3D-SBA-15 catalysts.

Table 1. Physical and chemical properties of 3D-SBA-15 and the catalysts.

Sample	S_{BET}^a ($\text{m}^2 \text{ g}^{-1}$)	V_p^b ($\text{cm}^3 \text{ g}^{-1}$)	D_p^c (nm)
3D-SBA-15	515.80	0.75	5.81
30PW/3D-SBA-15	396.55	0.59	5.99
50PW/3D-SBA-15	288.47	0.40	5.37
70PW/3D-SBA-15	184.27	0.20	4.27

^a Surface area, derived from BET equation;

^b Pore volume, obtained from the volume of nitrogen adsorbed at the relative pressure of 0.97;

^c D_p , average pore diameter of the calcined sample derived from BJH method using the following equation.

Successful loading of the $\text{H}_3\text{PW}_{12}\text{O}_{40}$ was confirmed by elemental analysis on the catalyst series (Table 2). This revealed a progressive increase in W content with nominal $\text{H}_3\text{PW}_{12}\text{O}_{40}$ loading. And as seen in Table 2, all sample show the similar pH values and Hammett acidity, thus acidity may play little role in changing the catalytic activities.

Table 2. Bulk composition and acid strength measurements of the series of PW/3D-SBA-15 catalysts.

Samples	Nominal $\text{H}_3\text{PW}_{12}\text{O}_{40}$ loading wt%	Actual $\text{H}_3\text{PW}_{12}\text{O}_{40}$ loading wt%	Bulk W (ICP) wt%	pH	Hammett acidity / H_0
30PW/3D-SBA-15	30	29.3	20.6	4.86	$-13.75 < \text{H}_0 < -11.35$
50PW/3D-SBA-15	50	49.6	34.9	4.67	$-13.75 < \text{H}_0 < -11.35$
70PW/3D-SBA-15	70	69.1	48.5	4.47	$-13.75 < \text{H}_0 < -11.35$
Pure PW	100	100.0	70.1	4.34	$-13.75 < \text{H}_0 < -11.35$

XRD

The SBA-15 monolithic material retains the pore structure of SBA-15. After calcination, the sample has three very distinct characteristic peaks on the small-angle XRD spectrum, corresponding to the (100), (110) and (200) crystal plane diffraction peaks of the hexagonal symmetry structure (The spatial point group: $p6mm$) indicates that the sample has a highly ordered mesoporous structure (Fig. 2a). As the loading increases, the intensity of the peak is gradually weakened, indicating that parts of the pores are occupied by the $\text{H}_3\text{PW}_{12}\text{O}_{40}$. Fig. 2(b) shows the wide-angle XRD patterns of 3D-SBA-15 and mPW/3D-SBA-15 catalysts. Also, the $\text{H}_3\text{PW}_{12}\text{O}_{40}$ was also analyzed as the reference. 3D-SBA-15 exhibits poor crystallinity even after high temperature treatments at 550 °C. The characteristic peaks of $\text{H}_3\text{PW}_{12}\text{O}_{40}$ on mPW/3D-SBA-15 catalysts become stronger with the increase of $\text{H}_3\text{PW}_{12}\text{O}_{40}$ loadings, indicating that the dispersion of $\text{H}_3\text{PW}_{12}\text{O}_{40}$ becomes poorer due to the excess loading.

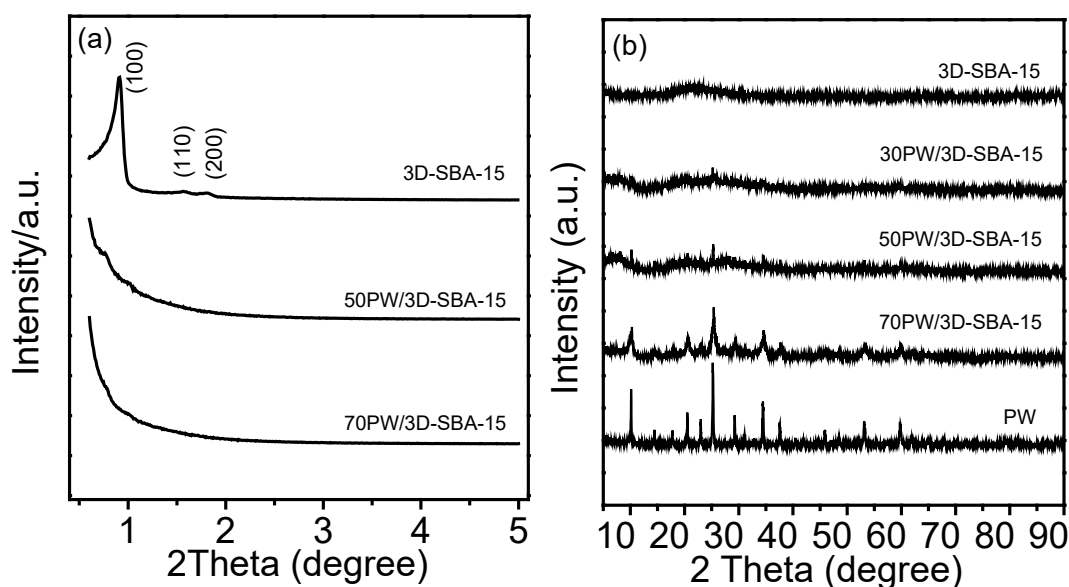


Fig. 2. Low-angle XRD patterns (a) and wide-angle XRD patterns (b) of 3D-SBA-15 and mPW/3D-SBA-15 catalysts.

FT-IR

In order to characterize the nanocatalyst and confirming immobilization of $\text{H}_3\text{PW}_{12}\text{O}_{40}$, FT-IR spectra of the 3D-SAB-15 and mPW/3D-SAB-15 were measured. For mPW/3D-SBA-15, there are two peaks at 1097 and 798 cm^{-1} which are related to stretching and bending vibration modes of Si–O–Si bonds. The peaks at 933, 959 and 1097 cm^{-1} are also observed, which are attributed to W–O–W and W=O and P–O stretching modes of $\text{H}_3\text{PW}_{12}\text{O}_{40}$, respectively. In addition, the band at about 1637 and 3455 cm^{-1} corresponds to the H–O–H bending vibration of the absorbed water [28].

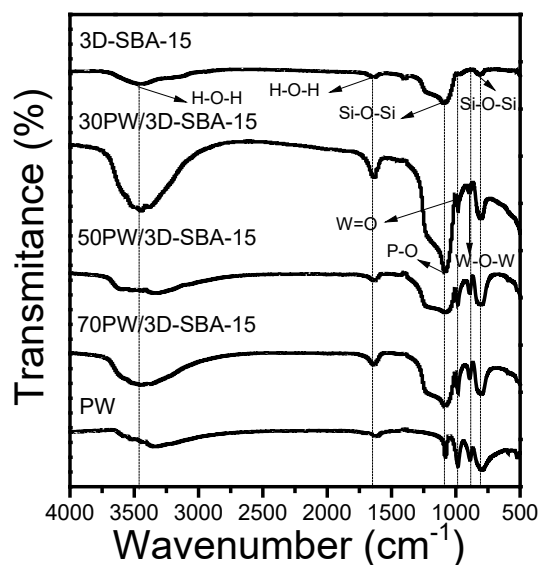
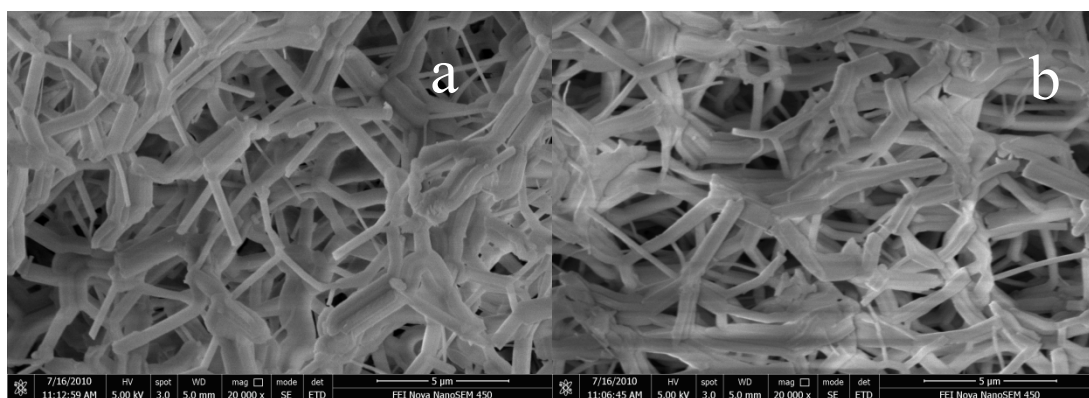


Fig. 3. FT-IR spectra of 3D-SBA-15 and mPW/3D-SBA-15.

SEM and TEM observations



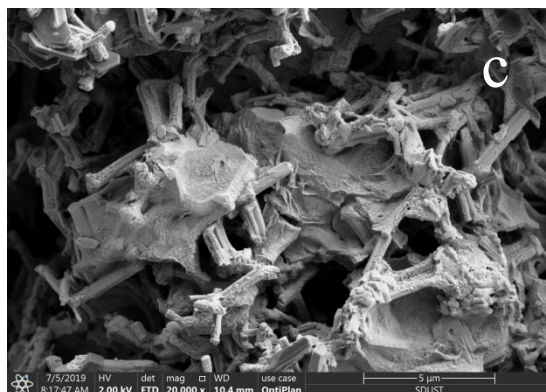


Fig. 4. SEM images of 3D-SBA-15 (a), 50PW/3D-SBA-15 (b) and 70PW/3D-SBA-15.

The SEM images reveal that the fiber-like components within 3D-SBA-15 are parallel-aligned and cross-linked with each other to form a periodically arranged framework in three dimensions throughout the whole sample (Fig. 4a) [24]. It can be seen that there is no change of morphology after the loading of 50 wt% $\text{H}_3\text{PW}_{12}\text{O}_{40}$ (Fig. 4b) due to its high dispersion (Fig. 2). When the loading amount reached 70 wt%, it was clearly observed that the phosphotungstic acid was piled up on the outside of the 3D-SBA-15 support without destruction of its three-dimensional and networked structure (Fig. 4c).

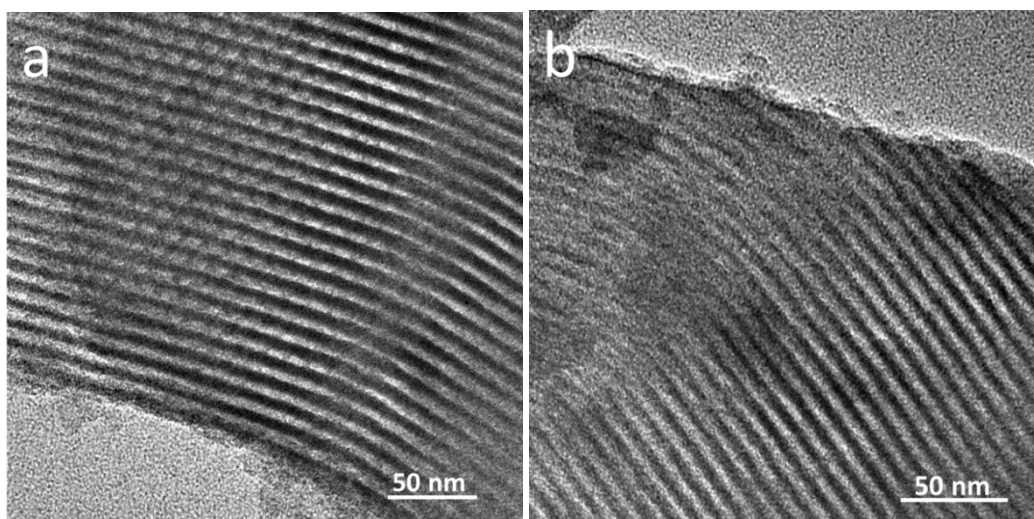


Fig. 5. TEM images of SBA-15(a) and 50PW/3D-SBA-15(b).

In order to clarify the pore architecture of catalysts, TEM observations have been carried out for 3D-SBA-15 and 50PW/3D-SBA-15, and the results were shown in Fig. 5. The typical ordered mesostructure with regular alignment of cylindrical pores along the (100) direction can be observed, exhibiting the ordered mesoporous 2D hexagonal arrays with uniform pore sizes of about 5.5 nm, which is in good agreement with the corresponding values determined by N_2 adsorption (Table 1). In addition, the incorporation of $\text{H}_3\text{PW}_{12}\text{O}_{40}$ into 3D-SBA-15 does not change the ordered mesopore structure with $p6mm$ hexagonal symmetry [27].

Thermogravimetric analysis

The TGA curves of $\text{H}_3\text{PW}_{12}\text{O}_{40}$ and 50PW/3D-SBA-15 are shown in Fig. 6. In Fig. 6(a), there are two obvious mass loss curves for $\text{H}_3\text{PW}_{12}\text{O}_{40}$. The first peak in the range of 30–236 °C with a weight loss of 4.1% can be attributed to the evaporation of adsorbed water. The second peak at 376 °C has a weight loss of 1.5%. For 50PW/3D-SBA-15, there is a continuous decrease from 30 °C to 168 °C with a weight loss of 5.8%, which may be due to more water being adsorbed in the sample (Fig. 6b). There is a weight loss at about 370 °C for both $\text{H}_3\text{PW}_{12}\text{O}_{40}$ and 50PW/3D-SBA-15, which corresponds to the removal of constitutional water, i.e. the H_3O^+ bound to the external oxygens of heteropoly acid [29].

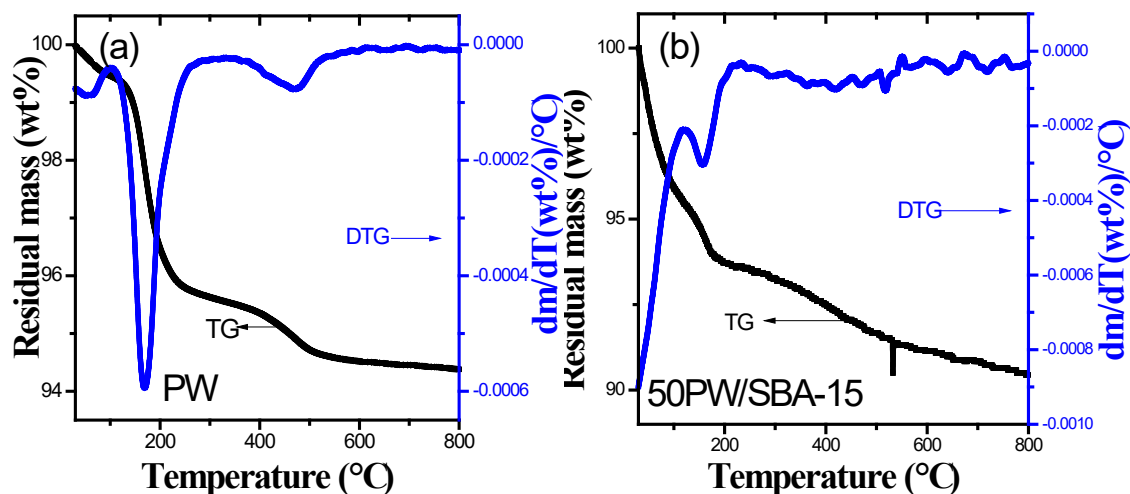


Fig. 6. Thermogravimetric analysis of $\text{H}_3\text{PW}_{12}\text{O}_{40}$ (a) and 50PW/3D-SBA-15 (b).

$\text{H}_3\text{PW}_{12}\text{O}_{40}$ /3D-SBA-15-catalyzed Mannich reaction

Effect of solvent

Developing green chemical methods is one of the most important purposes of organic synthesis at present. One of the fundamental challenges and ultimate goals for organic reactions is to perform the reaction under solvent-free condition or in environmentally friendly solvents. Here, in order to investigate the influence of the solvents, the model reaction of Mannich reaction was carried out through magnetic stirring method in two solvents and also under solvent-free condition at room temperature. As shown in Table 3, the catalytic performance decreases remarkably when $\text{C}_2\text{H}_5\text{OH}$ is used as solvent instead of H_2O in this work. As we know, the polarity of H_2O is larger than that of $\text{C}_2\text{H}_5\text{OH}$, and the higher polarity of solvent can lead to the enhanced catalytic activity, which is similar with the reported literature [30]. And the reaction under solvent-free condition finishes in 1.8 h with the yield of 93%, which shows higher activity than in the solvent of H_2O or $\text{C}_2\text{H}_5\text{OH}$. We can see that $\text{H}_3\text{PW}_{12}\text{O}_{40}$ /3D-SBA-15 is most effective under the solvent-free conditions, which allows Mannich reaction to be performed in a very simple, cheap and green manner.

Table 3. Effect of solvent on Mannich reaction of benzaldehyde, aniline and acetophenone^a

Entry	Solvent	Time (h)	Yield (%) ^b
1	Solvent-free	1.8	93.0
2	H_2O	7.0	93.0
3	$\text{C}_2\text{H}_5\text{OH}$	12.0	65.0

^aReaction conditions: benzaldehyde (10 mmol), aniline (10 mmol), acetophenone (10 mmol), magnetic stirring at room temperature, 50PW/3D-SBA-15 catalyst (0.5 g).

^bIsolated yield.

Effect of H₃PW₁₂O₄₀ loading

In order to evaluate effect of H₃PW₁₂O₄₀ loading on Mannich reaction, we investigated its efficiency over the model reaction among benzaldehyde, aniline and acetophenone. This reaction finishes in 4.5 h with the yield of 91.8% in the presence of 30PW/3D-SBA-15. With the increase of H₃PW₁₂O₄₀ loading, 50PW/3D-SBA-15 shows higher activity with yield of 93.0% in 1.8 h. This may be because the H₃PW₁₂O₄₀ loading of 30PW/3D-SBA-15 is too low, and the more H₃PW₁₂O₄₀ in 50PW/3D-SBA-15 can satisfy the reaction. For 70PW/3D-SBA-15, excessive H₃PW₁₂O₄₀ loading agglomerates and blocks the channels of 3D-SBA-15, resulting in the poor mass transfer during the reaction and low catalytic activity. Furthermore, the unloaded H₃PW₁₂O₄₀ was also investigated for this reaction, and it shows the lowest activity among all the catalyst, which is because the particle agglomeration of unloaded H₃PW₁₂O₄₀ limits its effective contact with the substrates compared with the supported catalysts. Thus, considering with the above results, 50PW/3D-SBA-15 is the best and used in the subsequent reaction.

Table 4. Effect of H₃PW₁₂O₄₀ loading on Mannich reaction of benzaldehyde, aniline and acetophenone^a

Entry	Catalyst	Time (h)	Yield (%) ^b
1	30PW/3D-SBA-15	4.5	91.8
2	50PW/3D-SBA-15	1.8	93.0
3	70PW/3D-SBA-15	5.0	94.2
4	Pure PW	10.0	80.0

^aReaction conditions: benzaldehyde (10 mmol), aniline (10 mmol), acetophenone (10 mmol), magnetic stirring at room temperature, solvent-free, mPW/3D-SBA-15 or H₃PW₁₂O₄₀ catalyst (0.5 g).

^bIsolated yield.

Table 5. Effect of amount of catalyst on Mannich reaction of benzaldehyde, aniline and acetophenone^a

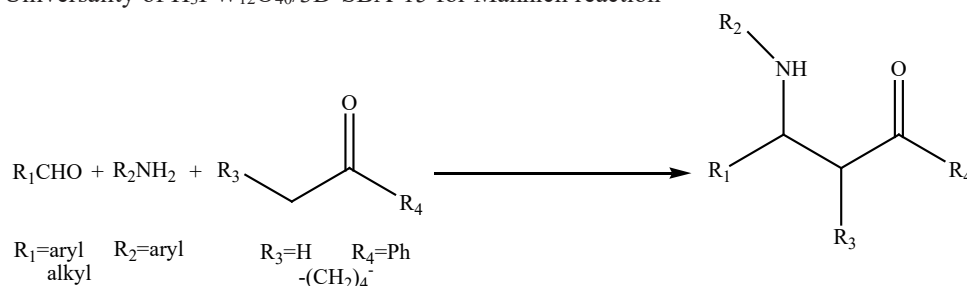
Entry	Amount of catalyst (g)	Time (h)	Yield (%) ^b
1	0.3	9.0	78.4
2	0.5	1.8	93.0
3	0.7	5.0	98.8

^aReaction conditions: benzaldehyde (10 mmol), aniline (10 mmol), acetophenone (10 mmol), magnetic stirring at room temperature, 50PW/3D-SBA-15 catalyst.

^bIsolated yield.

Effect of amount of catalyst

The catalytic effect of catalyst amount on the three-component Mannich reaction was investigated in the presence of the optimal 50PW/3D-SBA-15 catalyst. When the catalyst mass is 0.3 g, the reaction time is 9.0 h with the yield of 78.4%. With the increase of the amount of catalyst, this reaction can finish in 1.8 h with the yield of 93.0%, indicating that the more amount of catalyst is propitious to improve the activity of catalyst. However, the reaction time is 5.0 h in the presence of 0.7 g catalyst, which is much longer than that of 0.5 g catalyst. In the reaction system, 0.7 g of the 50PW/3D-SBA-15 catalyst increased the viscosity of the mixture of catalyst-substrate-solvent due to an excessive amount of solid powder catalyst, so that the mass transfer was decreased with the poor agitation, resulting in the prolonged reaction time. To comprehensively conclude our results, 0.5 g of the catalyst is the optimal amount for this reaction.

Table 6. Universality of H₃PW₁₂O₄₀/3D-SBA-15 for Mannich reaction

Entry	Aldehyde	Amine	Ketone		Time (h)	Yield (%)
	R ₁	R ₂	R ₃	R ₄		
1	Ph	Ph	H	Ph	1.8	93
2	4-ClC ₆ H ₄	Ph	H	Ph	12.0	90
3	4-CH ₃ C ₆ H ₄	Ph	H	Ph	26.0	92
4	4-CH ₃ OC ₆ H ₄	Ph	H	Ph	48.0	0
5	4-CH ₃ C ₆ H ₄	4-CH ₃ C ₆ H ₄	H	Ph	15.0	84
6	4-ClC ₆ H ₄	4-CH ₃ C ₆ H ₄	H	Ph	13.0	76
7	4-CH ₃ OC ₆ H ₄	4-CH ₃ C ₆ H ₄	H	Ph	10.0	75
8	Ph	4-CH ₃ C ₆ H ₄	H	Ph	24.0	63
9	4-ClC ₆ H ₄	4-CH ₃ C ₆ H ₄	-(CH ₂) ₄ -		31.0	58
10	Ph	4-CH ₃ C ₆ H ₄	-(CH ₂) ₄ -		18.0	62
11	Ph	Ph	-(CH ₂) ₄ -		22.0	51

^aReaction conditions: aldehyde (10 mmol), amine (10 mmol), ketone (10 mmol), 50PW/3D-SBA-15 catalyst (0.5 g), magnetic stirring at room temperature, solvent-free.

^bIsolated yield.

Universality of H₃PW₁₂O₄₀/3D-SBA-15 for Mannich reaction

Encouraged by the above results, a variety of aromatic aldehydes, amines and ketone were also examined, and the results are shown in Table 5. In the investigation of various aldehydes, both electron-withdrawing and electron-donating substituents could result in excellent yields, indicating the high generality of the aldehydes in this reaction (Table 5, entries 1–3). However, it was not beneficial to the formation of anisaldehyde. When para-substituted aniline was used as substrate, the reaction time is very long, possibly because of the steric hindrance of para-substituent, or other factors (Table 5, entries 5–10). Compared with cyclohexanone, acetophenone exhibits higher activity, probably because the benzene ring is conjugated and the π electron mobility is relatively strong, so the benzene ring has a better electron donating effect and can improve the reactivity. It makes its enol formation much faster than cyclohexanone.

Moreover, the H₃PW₁₂O₄₀/3D-SBA-15 catalyst was compared with the reported literatures for the Mannich reaction (Table 6). As seen, the 50PW/3D-SBA-15 catalyst system shows high activity, short reaction time, simple work-up and solvent-free, which further proves that this catalytic system is an efficient catalyst for Mannich reaction.

Table 7. Comparative study of various materials for Mannich reaction

Entry	Catalyst	Time(h)	Yield (%)	References
1	PPh ₃	12.0	52	[31]
2	Fe ₃ O ₄ -systeine MNPs	2.0	93	[32]
3	SO ₄ ²⁻ /TiO ₂	3.0	92	[33]
4	ZnI ₂	0.5-3.0	90	[34]
5	50PW/3D-SBA-15	1.8	93	This work

Reusability test of the catalyst

Facile catalyst recovery is an important advantage of any heterogeneous catalyst. After completion of the reaction, the $\text{H}_3\text{PW}_{12}\text{O}_{40}/3\text{D-SBA-15}$ catalyst was isolated by ethanol and acetone (1:1). After drying the isolated catalyst at 60 °C for 4 h, it was reused for Mannich reaction with fresh substrates, and the results are presented in Table 7. Apparently, the recovered catalyst could be reused for at least four successive times with almost the same catalytic activity, which shows high reusability.

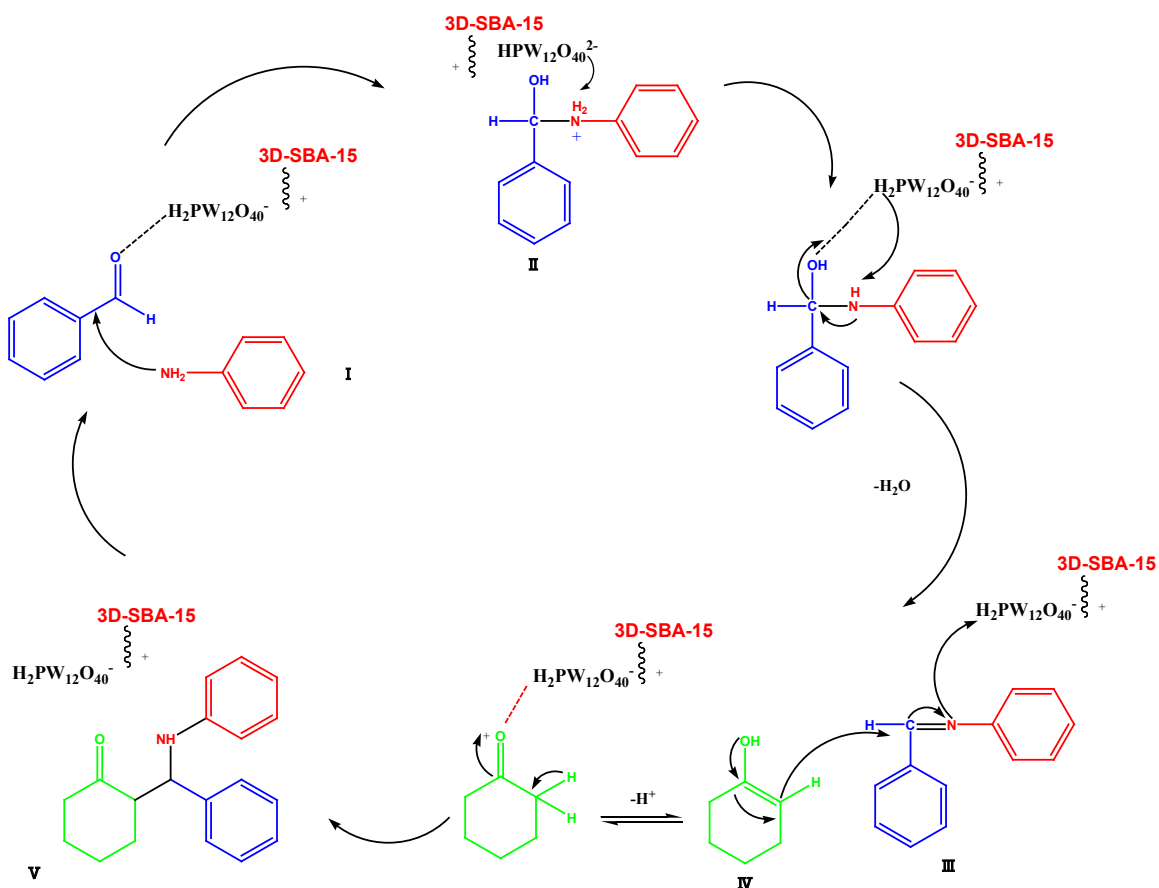
Table 8. Reusability of 50PW/3D-SBA-15 catalyst

Run	Fresh	1	2	3	4
Yield (%)	93	91	87	84	84

^aReaction conditions: benzaldehyde (10 mmol), aniline (10 mmol), acetophenone (10 mmol), magnetic stirring at room temperature, 50PW/3D-SBA-15 catalyst (0.5 g).

^bIsolated yield.

Proposed mechanism for Mannich reaction



Scheme 1. Proposed mechanism for Mannich reaction with PW/3D-SBA-15.

A proposed mechanism for Mannich reaction is shown in Scheme 1, which is consisted of three successive steps. In the first step, the carbonyl group of benzaldehyde is activated by $\text{H}_3\text{PW}_{12}\text{O}_{40}$ located on the surface of PW/3D-SBA-15 catalyst (intermediate I). A nucleophilic attack of aniline, through its lone pair of

electrons, to the carbonyl group of benzaldehyde will subsequently occur to produce intermediate (II). This intermediate passes through some rearrangement, transfer of proton and dehydration to give intermediate (III). In the second step or simultaneous with step (I), cyclohexanone is activated by the nanocatalyst and converted to enol form (IV). In the third and final step, the latter enol form attacks the iminium ion at carbon adjacent to positively charged nitrogen to give the expected β -aminocarbonyl compound (V) [28].

Conclusion

Nanocatalysts prepared by loading phosphotungstic acid on 3D-SBA-15 show a promising green route with high catalytic activity for the three components Mannich reaction of aldehydes, amines and ketones. This solvent-free catalyst system can contribute to a safer environment for green technology for facile preparation of β -aminocarbonyl compounds. It can be reused four times and still has good reactivity. The attractive features of this procedure were the mild reaction conditions, high yields, environment-friendly reaction profiles, recyclable and operational simplicity. All of which make it a useful and attractive strategy for the preparation of Mannich reaction.

Supporting Information

FTIR and ^1H NMR spectra of the synthesized compounds are available on the Journal's website.

Acknowledgements

The authors gratefully acknowledge the supports from National Natural Science Foundation of China (No. 21606146), Scientific Research Foundation of Shandong University of Science and Technology for Recruited Talents (No. 2016RCJJ005), Foundation of State Key Laboratory of High-efficiency Utilization of Coal and Green Chemical Engineering (No. 2018-K29), the Key Research and Development Plan of Shandong (No. 2018GGX104015), and the Applied Basic Research Programs of Qingdao (No. 17-1-1-23-jch).

References

1. Vaccaro, L. *Beilstein J. Org. Chem.* **2016**, *12*, 2763-2765.
2. Rafiee, E.; Eavani, S. *Green Chem.* **2011**, *13*, 2116.
3. Yang, H.; Dong, H.; Zhang, T.; Zhang, Q.; Zhang, G.; Wang, P.; Liu, Q. *Catal. Lett.* **2018**, *149*, 778-787.
4. Yang, L.; Xu, L.W.; Xia, C.G. *Tetrahedron Lett.* **2005**, *46*, 3279-3282.
5. Yan, X.; Chen, J.; Xue, Q.; Miele, P. *Micropor. Mesopor. Mat.* **2010**, *135*, 137-142.
6. Hussain, M.; Liu, J.; Zhang, Z.; Hu, M.; Li, Y.; Min, X. *ChemistrySelect* **2018**, *3*, 8787-8792.
7. Yeszhanov, A.B.; Mashentseva, A.A.; Korolkov, I.V.; Gorin, Y.G.; Kozlovskiy, A.L.; Zdorovets, M.V. *Chem. Pap.* **2018**, *72*, 3189-3194.
8. Pettignano, A.; Bernardi, L.; Fochi, M.; Geraci, L.; Robitzer, M.; Tanchoux, N.; Quignard, F. *New J. Chem.* **2015**, *39*, 4222-4226.
9. Sawant, D.P.; Justus, J.; Balasubramanian, V.V.; Ariga, K.; Srinivasu, P.; Velmathi, S.; Halligudi, S.B.; Vinu, A. *Chem.* **2008**, *14*, 3200-3212.
10. Okuhara, T.; Mizuno, N.; Misono, M. *Appl. Catal. A-Gen.* **2001**, *222*, 63-77.
11. Rafiee, E.; Joshaghani, M.; Eavani, S.; Rashidzadeh, S. *Green Chem.* **2008**, *10*, 982-989.
12. Sahoo, S.; Joseph, T.; Halligudi, S.B. *J. Mol. Catal. A: Chem.* **2006**, *244*, 179-182.

13. Zhang, Y.; Zhao, Y.; Xia, C. *J. Mol. Catal. A: Chem.* **2009**, 306, 107-112.
14. Zhang, H.; Mifsud, M.; Tanaka, F.; Barbas Iii, C.F. *J. Am. Chem. Soc.* **2006**, 128, 9630-9631.
15. Timofeeva, M.N. *Appl. Catal. A-Gen* **2003**, 256, 19-35.
16. Wang, Y.; Satyavolu, N.S.R.; Lu, Y. *Curr. Opin. Colloid Interface Sci.* **2018**, 38, 158-169.
17. Chen, G.; Zhang, X.; Guo, C.; Yuan, G. *Russ. J. Phys. Chem. A* **2010**, 84, 2247-2253.
18. Hu, B.; Liu, H.; Tao, K.; Xiong, C.; Zhou, S. *J. Phys. Chem. C* **2013**, 117, 26385-26395.
19. Dong, C.; Li, X.; Wang, A.; Chen, Y.; Liu, H. *Catal. Commun.* **2017**, 100, 219-222.
20. Dan, H.; Dong, X.; Lu, X.; Ding, Y. *J. Sol-Gel Sci. Technol.* **2017**, 81, 782-790.
21. Schwanke, A.; Favero, C.; Balzer, R.; Bernardo-Gusmão, K.; Pergher, S. *J. Braz. Chem. Soc.* **2017**, 29, 328-333.
22. Yang, Q.; Gu, F.; Tang, Y.; Zhang, H.; Liu, Q.; Zhong, Z.; Su, F. *RSC Adv.* **2015**, 5, 26815-26822.
23. Zhou, Y.; Lin, W.G.; Yang, J.; Gao, L.; Lin, N.; Yang, J.Y.; Hou, Q.; Wang, Y.; Zhu, J.H. *J. Colloid Interface Sci.* **2011**, 364, 594-604.
24. Liu, Q.; Tian, Y. *Int. J. Hydrogen Energy* **2017**, 42, 12295-12300.
25. Cele, Z.E.D.; Pawar, S.A.; Naicker, T.; Maguire, G.E.M.; Arvidsson, P.I.; Kruger, H.G.; Govender, T. *Eur. J. Org. Chem.* **2014**, 2014, 2253-2260.
26. Liu, Q.; Zhang, Z. *Catal. Sci. Technol.* **2019**, 9, 4821-4834.
27. Wang, H.; Gao, X.; Wang, Y.; Wang, J.; Niu, X.; Deng, X. *Ceram. Int.* **2012**, 38, 6931-6935.
28. Kooti, M.; Kooshki, F.; Nasiri, E.; Sedeh, A.N. *J. Iran. Chem. Soc.* **2018**, 15, 943-953.
29. Armatas, G.S.; Katsoulidis, A.P.; Petrakis, D.E.; Pomonis, P.J. *J. Mater. Chem.* **2010**, 20, 8631-8638.
30. Zhu, X.; Chen, C.; Yu, B.; Wu, Y.; Zhang, G.; Zhang, W.; Gao, Z. *Catal. Sci. Technol.* **2015**, 5, 4346-4349.
31. Hussain, M.; Liu, J.; Zhang, Z.; Hu, M.; Li, Y.; Min, X. *ChemistrySelect* **2018**, 3, 8787-8792.
32. Gawande, M.B.; Velinho, A.; Nogueira, I.D.; Ghumman, C.A.A.; Teodoro, O.M.N.D.; Branco, P.S. *RSC Adv.* **2012**, 2, 6144-6149.
33. Eftekhari-Sis, B.; Hashemi, M.M.; Farmad, F. *Synth. Commun.* **2009**, 39, 4441-4453.
34. Azizi, N.; Torkiyan, L.; Saidi, M.R. *Org. Lett.* **2006**, 8, 2079-2082.